3. Duc, P.-A., Brinks, E., Wink, J. E. & Mirabel, I. F. Gas segregation in the interacting system Arp 105. *Astron. Astrophys.* **326,** 537–553 (1997).
4. Duc, P.-A. & Mirabel, I. G. Young tidal dwarf galaxies around the gas-rich disturbed lenticular NGC 5291. *Astron. Astrophys.* **333,** 813–826 (1998).
5. Brouillet, N., Henkel, C. & Baudry, A. Detection of an intergalactic molecular complex? *Astron. Astrophys.* **262,** L5–L8 (1992).
6. Walter, F. & Heithausen, A. The discovery of a molecular complex in the tidal arms near NGC 3077. *Astrophys. J.* **519,** L69–L72 (1999).
7. Smith, B. J. & Higdon, J. L. A search for CO(1–0) emission from the tidal structures of interacting and merging galaxies. *Astron. J.* **108,** 837–843 (1994).
8. Smith, B. J., Struck, C., Kenney, J. D. P. & Jogee, S. The molecule-rich tail of the peculiar galaxy NGC 2782 (Arp 215). *Astron. J.* **117,** 1237–1248 (1999).
9. Zwicky, F. Multiple galaxies. *Ergenisse Exakten Naturwissenschaften* **29,** 344–385 (1956).
10. Schweizer, F. in *Structure and Properties of Nearby Galaxies* (eds Berkhuijsen, E. M. & Wielebinski, R.) 279–284 (Riedel, Dordrecht, 1978).
11. Hibbard, J. E. & van Gorkom, J. H. HI, HII, and R-Band observations of a galactic merger sequence. *Astron. J.* **111,** 655–695 (1996).
12. Duc, P.-A. & Mirabel, I. F. in *Galaxy Interactions at Low and High Redshift* (eds Barnes, J. & Sanders, D.) 61–70 (IAU Symp. 186, Kluwer, Dordrecht, 1997).
13. Barnes, J. E. & Hernquist, L. Formation of dwarf galaxies in tidal tails. *Nature* **360,** 715–717 (1992).
14. Duc, P.-A. *et al.* The interacting system NGC 2992/3 (Arp 245). *Astron. J.* (submitted).
15. Taylor, C. L., Kobulnicky, H. A. & Skillman, E. D. CO emission in low-luminosity, HI-rich galaxies. *Astron. J.* **116,** 2746–2756 (1998).
16. Kennicutt, R. C. Jr Star formation in galaxies along the Hubble sequence. *Annu. Rev. Astron. Astrophys.* **36,** 189–232 (1998).
17. Guélin, M. *et al.* 1.3 mm emission in the disk of NGC 891: Evidence of cold dust. *Astron. Astrophys.* **279,** L37–L40 (1993).
18. Braine, J., Combes, F. & Van Driel, W. NGC 4414: A flocculent galaxy with a high gas surface density. *Astron. Astrophys.* **280,** 451–467 (1993).
19. Hollenbach, D. & MCKee, C. F. Molecule formation and infrared emission in fast interstellar shocks. III—results for J shocks in molecular clouds. *Astrophys. J.* **342,** 306–336 (1989).
20. Neininger, N., Guélin, M., Garcia-Burillo, S., Zylka, R. & Wielebinski, R. Cold dust and molecular line emission in NGC 4565. *Astron. Astrophys.* **310,** 725–736 (1996).
21. Dumke, M. *et al.* the interstellar medium in the edge-on galaxy NGC 5907. Cold dust and molecular line emission. *Astron. Astrohys.* **325,** 124–134 (1997).
22. Braine, J. *et al.* Gas and dust in the active spiral galaxy NGC 3079. *Astron. Astrophys.* **326,** 963–975 (1997).
23. Sage, L. J. The properties and origins of molecular gas in the lenticular galaxies NGC 404, 4710 and 5195. *Astron. Astrophys.* **239,** 125–136 (1990).
24. Arp, H. Atlas of peculiar galaxies. *Astrophys. J. Suppl. Ser.* **14,** 1–20 (1966).
25. Fritze-v.Alvensleben, U. & Duc, P.-A. in *The Magellanic Clouds and other Dwarf Galaxies* (eds Braun, J. M. & Richtler, T.) 141–145 (Proceedings of the Workshop of the Graduiertenkolleg Bonn-Bochum, Shaker, Aachen, 1998).

Correspondence and requests for materials should be addressed to J.B. (e-mail: Jonathan.Braine@observ.u-bordeaux.fr).

Geometric quantum computation using nuclear magnetic resonance

Jonathan A. Jones*†, Vlatko Vedral*, Artur Ekert* & Giuseppe Castagnoli‡

* *Centre for Quantum Computation, Clarendon Laboratory, Parks Road, Oxford OX1 3PU, UK*
† *Oxford Centre for Molecular Sciences, New Chemistry Laboratory, South Parks Road, Oxford OX1 3QT, UK*
‡ *Elsag, Via Puccini 2, 1615 Genova, Italy*

A significant development in computing has been the discovery[1] that the computational power of quantum computers exceeds that of Turing machines. Central to the experimental realization of quantum information processing is the construction of fault-tolerant quantum logic gates. Their operation requires conditional quantum dynamics, in which one sub-system undergoes a coherent evolution that depends on the quantum state of another sub-system[2]; in particular, the evolving sub-system may acquire a conditional phase shift. Although conventionally dynamic in origin, phase shifts can also be geometric[3,4]. Conditional geometric (or 'Berry') phases depend only on the geometry of the path executed, and are therefore resilient to certain types of errors; this suggests the possibility of an intrinsically fault-tolerant way of performing quantum gate operations. Nuclear magnetic resonance techniques have already been used to demonstrate both simple quantum information processing[5–9] and geometric phase shifts[10–12]. Here we combine these ideas by performing a nuclear magnetic resonance experiment in which a conditional Berry phase is implemented, demonstrating a controlled phase shift gate.

Any quantum computation can be built out of simple operations involving only one or two quantum bits (qubits)[13]. A particularly simple two-qubit gate in many experimental implementations, such as nuclear magnetic resonance (NMR)[14], is the controlled phase shift. This may be achieved using a conditional Berry phase, and thus quantum geometrical phases can form the basis of quantum computation. We will use spin half nuclei as an example to demonstrate the feasibility of this approach, but the basic idea is general. In our experiments the state of one spin determines the Berry phase acquired by the other spin.

Suppose that a spin half nucleus undergoes a conical evolution with cone angle θ. Then the Berry phase is simply $\gamma = \pm\frac{1}{2}\Omega = \pm\pi(1-\cos\theta)$ where the $\pm$ signs depend on whether the system is in the eigenstate aligned with or against the field, and Ω is the solid angle subtended by the conical circuit. We note that any deformation of the path of the spin which preserves this solid angle leaves the phase unchanged. Thus the phase is not affected by the speed with which the path is traversed; nor is it very sensitive to random fluctuations about the path.

Berry phases can be conveniently demonstrated in an NMR experiment[15] by working in a rotating frame. We consider an ensemble of spin half particles in a magnetic field, B_0, aligned along the z-axis; their precession frequency is then given by the Larmor frequency, ω_0. If the spins are irradiated by a circularly polarized radio-frequency field, B_1, at a frequency ω_{rf}, the total hamiltonian (neglecting relaxation) may be written in the rotating frame as $H = (\omega_0 - \omega_{rf})I_z + \omega_1 I_x$, where, following conventional NMR practice, the hamiltonian is described in product operator notation[16] and the field strengths are written in terms of their corresponding Larmor frequencies.

When $|\omega_1| \ll |\omega_0 - \omega_{rf}|$ the hamiltonian lies close to the z-axis, while when $|\omega_1| \gg |\omega_0 - \omega_{rf}|$, the hamiltonian lies close to the x-axis. If radio-frequency radiation is applied far from resonance, the system is effectively quantized along the z-axis, and if the radio frequency is swept towards resonance ($\omega_{rf} = \omega_0$), the effective hamiltonian rotates from the z-axis towards the x-axis. If the frequency sweep is applied adiabatically then the spin will follow the hamiltonian. Next, a circular motion can be imposed by adiabatically varying the phase of the radio frequency. When the hamiltonian returns to the x-axis the frequency sweep may be reversed, so that the spin returns to its original state, aligned along the z-axis. The Berry phase acquired in this cyclic process is $\pm\pi$. If the radio-frequency field is not swept all the way to resonance, but only to some final value ω_f, the hamiltonian ends at some angle to the z-axis, and so circuits with arbitrary cone angles can be implemented. A similar case occurs if the frequency sweep is replaced by an amplitude sweep, in which the radio frequency is always applied away from resonance, and its amplitude is raised smoothly from zero to some final value, ω_1.

This situation arises naturally in a system of two weakly coupled spins, I and S. For simplicity we consider a heteronuclear system, so that ω_I and ω_S are very different, and only one spin (say I) is close to resonance. The two transitions of I (corresponding to the two possible states of spin S) will be split by $\pm\pi J$, and so will have different resonance offsets. After an amplitude sweep the orientation of the effective hamiltonian depends on the resonance offset, and so θ (and hence the Berry phase acquired) will depend on the state of spin S. This permits a conditional Berry phase to be applied to spin I, where the size of the phase shift is controlled by spin S. If the radio frequency is applied at a frequency δ (measured in Hz)

away from the transition frequency of spin I when spin S (the control spin) is in state 0, and ν_1 is the maximum radio-frequency field strength (also in Hz), then the differential Berry phase shift

$$\Delta\gamma = \gamma_1 - \gamma_0 = \pm\pi\left[\frac{\delta + J}{\sqrt{(\delta + J)^2 + \nu_1^2}} - \frac{\delta}{\sqrt{\delta^2 + \nu_1^2}}\right]$$

depends only on δ, ν_1 and J; it is independent of how the process is carried out as long as it is slow enough to be adiabatic, but rapid compared with the decoherence times (T_1 and T_2).

In addition to the geometric phases, there will also be additional dynamic phases, which do depend on experimental details. In principle these could be calculated and corrected for, but this is not practical as a result of B_1 inhomogeneity. The radio-frequency field strength will vary over the sample, and so different nuclei will acquire different dynamic phases; averaging over the sample will result in extensive dephasing. This can be overcome using a conventional spin echo approach: the pulse sequence is applied twice, with the second application surrounded by a pair of 180° pulses applied to spin I. This has the effect of completely refocusing the dynamic phase, and thus refocusing any inhomogeneity in it. We note that this approach will only be successful if the dynamic phase terms are the same during the two halves of the spin echo, and thus it is important that any variation in these terms occurs on a timescale that is long compared with the echo time. In our experiments minor variations in the dynamic phase arising from the effects of molecular diffusion within the slightly inhomogeneous B_1 field are visible as a small loss in signal intensity. Similarly it is important to ensure that refocusing pulses are applied reliably, which is relatively simple within NMR. These issues must be considered when seeking to apply this approach with other experimental techniques.

This procedure would also cancel out the geometric phase, but this can be sidestepped by performing the radio-frequency phase sweep in the opposite direction, thus negating the geometric phase, so that the two geometric terms add together while the dynamic phases cancel out. Cancellation of dynamic phases arising from the natural evolution of spin S, could also be achieved by incorporating the sequence within another spin echo, involving 180° pulses applied to S. Similarly, in more complex spin systems, contributions to the geometric phase which depend on the states of other spins can be cancelled by the judicious application of further spin echoes. It might seem that this approach would require an exponentially large number of refocusing pulses, but this is not true, as nuclear spin–spin coupling is a local effect, so that couplings between distant nuclei can be safely neglected. It should also be possible to use efficient refocusing schemes[17] based on Hadamard matrices, thus allowing the number of refocusing pulses to be further reduced.

In order to measure the sizes of γ_0 and γ_1 it is convenient to apply the Berry phase shifts to a spin I in a coherent superposition of states, created by an initial 90° pulse. The pulse sequence (Fig. 1) then generates Berry phases that are determined by examining the final phases of the magnetization. As the two states of spin I acquire equal and opposite phases, and the pulse sequence contains two separate periods in which phase shifts are generated, the total phase change observed is 4γ, with a maximum value of 720°. A range of controlled Berry phases can be generated by choosing appropriate values of δ and ν_1 (J is fixed by the chemical system). For a given value of δ/J the controlled phase will rise and then fall as ν_1 is increased. This approach will be most robust when the desired $\Delta\gamma$ occurs at the maximum of this curve, as the dependence on the size of δ is then reduced to second order. For the particular case of a controlled π shift, the basis of the controlled-NOT gate[14], this occurs at $\delta = 1.058J$ and $\nu_1 = 2.112J$.

NMR experiments were performed at 25 °C using a homebuilt 500 MHz (^{1}H frequency) NMR spectrometer at the OCMS, with two power ranges for ^{1}H pulses. Hard pulses were applied using high power ($\nu_1 < 25.8$ kHz), while adiabatic sweeps were performed using low power ($\nu_1 < 774$ Hz). Radio-frequency amplitude and phase-calibration tables (available on most modern NMR spectrometers) permit the radio-frequency power level to be varied in a phase-coherent manner. The sample was prepared by dissolving 100 mg of 99% ^{13}C-labelled $CHCl_3$ in 0.2 ml of 99.96% $CDCl_3$, and placing this in a Shigemi microtube. The single ^{1}H nucleus was used as spin I, while the ^{13}C nucleus was used as spin S; for this system $J_{IS} = 209.2$ Hz. Spin–spin relaxation times (measured using Carr–Purcell–Meiboom–Gill sequences and averaging over the two components of each doublet) were 3.9 s for ^{1}H and 0.3 s for ^{13}C; the spin–lattice relaxation times (measured by inversion-recovery) were 7.6 s for ^{1}H and 25.3 s for ^{13}C. Experiments were performed with $\delta = 221.3$ Hz, and ν_1 was varied between zero and its maximum value. Amplitude and phase sweeps were implemented using 200 linear steps of 100 μs, giving a total pulse sequence length of about 120 ms. The phases of the two ^{1}H resonances were determined by fitting the free induction decay using home-written software. Reference phases were obtained as described in Fig. 1 (legend). The results are shown in Fig. 2; clearly the measured phases lie close to the theoretically predicted values. The controlled Berry phase rises smoothly to a broad maximum at 180°, and then slowly falls back towards zero. In order to investigate the effects of a breakdown in the adiabatic criterion, some measurements were repeated with faster sweeps. With a sweep step size of 50 μs (data not shown) the

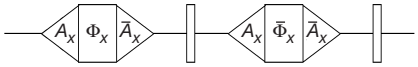

Figure 1 Pulse sequence used to demonstrate controlled Berry phases. Triangles indicate adiabatic radio-frequency amplitude sweeps, from 0 to ν_1 (A_x) or from ν_1 to 0 ($\bar{A}_x$); rectangles indicate slow rotations of the radio-frequency phase at constant amplitude. The phase rotation runs from 0° to 360° (Φ_x) or from 360° to 0° ($\bar{\Phi}_x$). Narrow rectangles correspond to hard 180°$_y$ pulses. As the absolute phase of an NMR signal is undefined, it is essential to obtain a reference signal against which experimental phases can be measured. The simplest approach is to use the signal from a single 90° pulse, and a more subtle approach is to use this pulse sequence with the $\bar{\Phi}_x$ sequence replaced by Φ_x. In principle these should give the same result, but in practice minor differences are seen as a result of radio-frequency inhomogeneity and the effects of the long radio-frequency pulses on the NMR probe and pre-amplifier.

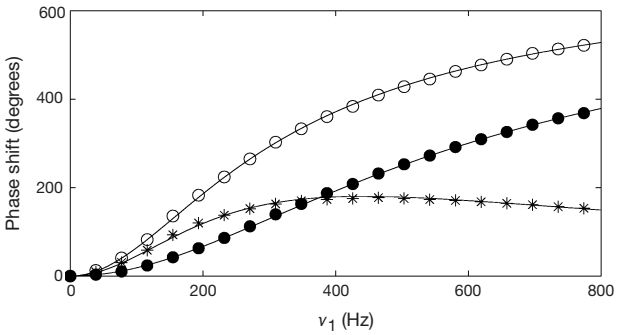

Figure 2 Experimental values for the Berry phases γ_0, γ_1, and the controlled Berry phase difference, $\Delta\gamma$, as a function of the maximum radio-frequency field strength ν_1. Experimental points are shown by filled circles (γ_0), empty circles (γ_1) and stars ($\Delta\gamma$); theoretical values are shown as smooth curves. Variability in the experimental points (estimated by repetition) was about ±2°; in a few cases the deviation of the measured data points from their theoretical values was greater than this, indicating the existence of as yet unidentified systematic errors. The signal strength observed after a phase gate was about 90% of that observed without a phase gate. This signal loss of about 10% is too great to arise simply from relaxation; more detailed experiments (data not shown) suggest that the main source of signal loss is the effect of diffusion. When considering the overall fidelity of the gate it is also necessary to include effects arising from spin S; these are dominated by the relatively rapid spin–spin (T_2) relaxation of the ^{13}C nucleus.

results were similar to, but not quite as good as, those obtained with the slower sweep. Below 50 μs the loss of adiabaticity is severe and major distortions are observed. The step size should not be increased too far beyond the adiabatic threshold, as this will increase the effects of decoherence.

The conditional Berry phase gate demonstrated here depends only on the geometry of the path, and is completely independent of how the motion is performed as long as it is adiabatic; hence this kind of computation may be called geometric quantum computation. While this approach has no particular advantage over more conventional methods in NMR quantum computation, the basis idea is general, and could be applied in other implementations. Some of the methods described here have been partly covered in previous theory papers (such as refs 18 and 19), but there have been no previous experimental demonstrations. This new approach to quantum gates may become important, as it is naturally resilient to certain types of errors. In particular, suppose that the qubit, in addition to the circular motion which implements the geometric phase, also undergoes a random motion about its path due to some unwanted interaction with the environment. Such noisy motion leaves the total area approximately unchanged (although it changes details of the path), and so will not be reflected in the final Berry phase. Geometric phases thus offer the potential of performing quantum computations in a manner which is naturally tolerant of some types of fault. Further generalizations to non-abelian Berry phases, if implemented, may open entirely new possibilities for robust quantum information processing[20,21]. □

Received 22 July; accepted 14 December 1999.

1. Shor, P. W. Polynomial-time algorithms for prime factorization and discrete logarithms on a quantum computer. *SIAM Rev.* **41,** 303–332 (1999).
2. Barenco, A., Deutsch, D., Ekert, A. & Jozsa, R. Conditional quantum dynamics and logic gates. *Phys. Rev. Lett.* **74,** 4083–4086 (1995).
3. Berry, M. V. Quantal phase factors accompanying adiabatic changes. *Proc. R. Soc. Lond. A* **392,** 45–57 (1984).
4. Shapere, A. & Wilczek, F. *Geometric Phases in Physics* (World Scientific, Singapore, 1989).
5. Cory, D. G., Fahmy, A. F. & Havel, T. F. Ensemble quantum computing by NMR spectroscopy. *Proc. Natl Acad. Sci. USA* **94,** 1634–1639 (1997).
6. Gershenfeld, N. A. & Chuang, I. L. Bulk spin-resonance quantum computation. *Science* **275,** 350–356 (1997).
7. Jones, J. A. & Mosca, M. Implementation of a quantum algorithm on a nuclear magnetic resonance quantum computer. *J. Chem. Phys.* **109,** 1648–1653 (1998).
8. Chuang, I. L., Gershenfeld, N. & Kubinec, M. Experimental implementation of fast quantum searching. *Phys. Rev. Lett.* **80,** 3408–3411 (1998).
9. Cory, D. G., Price, M. D. & Havel, T. F. Nuclear magnetic resonance spectroscopy: An experimentally accessible paradigm for quantum computing. *Physica D* **120,** 82–101 (1998).
10. Suter, D., Chingas, G., Harris, R. & Pines, A. Berry's phase in magnetic resonance. *Mol. Phys.* **61,** 1327–1340 (1987).
11. Goldman, M., Fleury, V. & Guéron, M. NMR frequency shift under sample spinning. *J. Magn. Reson. A* **118,** 11–20 (1996).
12. Jones, J. A. & Pines, A. Geometric dephasing in zero-field magnetic resonance. *J. Chem. Phys.* **106,** 3007–3016 (1997).
13. Deutsch, D., Barenco, A. & Ekert, A. Universality in quantum computation. *Proc. R. Soc. Lond. A* **449,** 669–677 (1995).
14. Jones, J. A., Hansen, R. H. & Mosca, M. Quantum logic gates and nuclear magnetic resonance pulse sequences. *J. Magn. Reson.* **135,** 353–360 (1998).
15. Ernst, R. R., Bodenhausen, G. & Wokaun, A. *Principles of Nuclear Magnetic Resonance in One and Two Dimensions* (Clarendon, Oxford, 1987).
16. Sørensen, O. W., Eich, G. W., Levitt, M. H., Bodenhausen, G. & Ernst, R. R. Product operator-formalism for the description of NMR pulse experiments. *Prog. Nucl. Magn. Reson. Spectrosc.* **16,** 163–192 (1983).
17. Jones, J. A. & Knill, E. Efficient refocussing of one spin and two spin interactions for NMR quantum computation. *J. Magn. Reson.* **141,** 322–325 (1999).
18. Pellizzari, T., Gardiner, S. A., Cirac, J. I. & Zoller, P. Decoherence, continuous observation, and quantum computing: a cavity QED model. *Phys. Rev. Lett.* **75,** 3788–3791 (1995).
19. Averin, D. V. Adiabatic quantum computation with Cooper pairs. *Solid State Commun.* **105,** 659–664 (1998).
20. Kitaev, A. Y. Fault tolerant quantum computation with anyons. Preprint http://arxiv.org/quant-ph/9707021.
21. Preskill, J. Fault tolerant quantum computation. Preprint http://arxiv.org/quant-ph/9712048.

Acknowledgements

We thank N. Soffe for helpful discussions. J.A.J. and A.E. thank the Royal Society of London and Starlab (Riverland NV) for financial support.

Correspondence and requests for materials should be addressed to J.A.J. (e-mail: jonathan.jones@qubit.org).

Reduction in the surface energy of liquid interfaces at short length scales

C. Fradin*, A. Braslau*, D. Luzet*, D. Smilgies†, M. Alba*, N. Boudet†, K. Mecke‡ & J. Daillant*§

** Service de Physique de l'Etat Condensé, CEA Saclay, F-91191 Gif-sur-Yvette Cedex, France*

† European Synchrotron Radiation Facility, BP 220, F-38043 Grenoble Cedex, France

‡ Theoretische Physik, Bergische Universität Wuppertal, D-42097 Wuppertal, Germany

§ LURE, Centre Universitaire Paris-sud, bâtiment 209D, PB 34, F-91898 Orsay Cedex, France

Liquid–vapour interfaces, particularly those involving water, are common in both natural and artificial environments. They were first described as regions of continuous variation of density[1], caused by density fluctuations within the bulk phases[2–4]. In contrast, the more recent capillary-wave model[5,6] assumes a step-like local density profile across the liquid–vapour interface, whose width is the result of the propagation of thermally excited capillary waves. The model has been validated for length scales of tenths of micrometres and larger[7,8], but the structure of liquid surfaces on submicrometre length scales—where the capillary theory is expected to break down—remains poorly understood. Here we report grazing-incidence X-ray scattering experiments that allow for a complete determination of the free surface structure and surface energy for water and a range of organic liquids. We observe a large decrease of up to 75% in the surface energy of submicrometre waves that cannot be explained by capillary theory, but is in accord with the effects arising from the non-locality of attractive intermolecule interactions as predicted by a recent density functional theory[9]. Our data, and the results of comparable measurements on liquid solutions, metallic alloys, surfactants, lipids and wetting films should thus provide a stringent test for any new theories that attempt to describe the structure of liquid interfaces with nanometre-scale resolution.

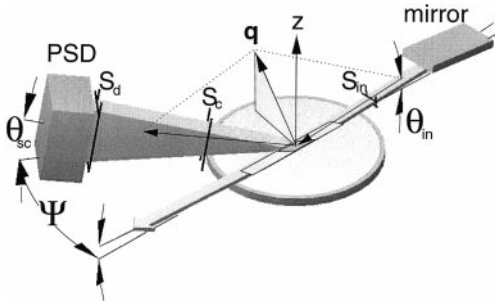

Figure 1 Schematic view of the experiment. The Teflon trough (inner diameter is 330 mm) is mounted on an active antivibration system under a helium atmosphere saturated with the vapour of the liquid under study. The monochromatic incident beam is first extracted from the polychromatic beam of the undulator source using a two-crystal diamond (111) monochromator. Higher harmonic light is eliminated using two platinum-coated glass mirrors, also used to fix the grazing angle of incidence θ_{in}. The incident and scattered beams travel through vacuum paths and the scattered signal is collected in a vertically mounted position sensitive detector (PSD). The size of the incident beam is fixed by a 265 μm × 250 μm slit, S_{in}. The horizontal resolution of the experiment is fixed by the slits S_c, 380 μm in width and S_d, 545 μm in width, placed at 213 mm and 844 mm from the sample respectively, as well as by the illuminated area seen by the detector (dark grey parallelogram in centre of circle). The scattered beam is defined by the angles Ψ and θ_{sc}. **q** is the wavevector transfer.